Shear Stress Induces a Pro-Inflammatory Phenotype in Human Monocyte-Derived Macrophages

Elysa Jui[1], Griffin Kingsley[1], Hong Kim T. Phan[1], Kavya L. Singampalli[1,2], Ravi K. Birla[3,4], Jennifer P. Connell[1], Sundeep G. Keswani[3,4], K. Jane Grande-Allen[1]

Affiliations

[1]Department of Bioengineering, Rice University, Houston, TX, United States

[2]Medical Scientist Training Program, Baylor College of Medicine, Houston, TX, United States

[3]Department of Surgery, Baylor College of Medicine, Houston, TX, United States

[4]Division of Pediatric Surgery, Department of Surgery, Texas Children's Hospital, Houston, TX, United States

Abbreviated title

Shear stress-induced MDM phenotype

Address for correspondence

K. Jane Grande-Allen, Ph.D.

Department of Bioengineering

Rice University

6100 Main St., MS 142

Houston, TX 77005

Phone: 713-348-3704

Email: grande@rice.edu

Abstract

Macrophages are innate immune cells that are known for their diverse phenotypes and plasticity. They switch between pro-inflammatory (M1) and anti-inflammatory/pro-fibrotic (M2) phenotypes depending on surrounding microenvironmental cues, which have been implicated in disease outcomes. Although considerable research has been focused on macrophage response to biochemical cues and mechanical signals, there is a scarcity of knowledge surrounding their behavior in response to shear stress. Animal studies have shown that shear stress modulates macrophage activation; however it is difficult to determine the specific signals that macrophages release in response to shear *in vivo*, due to the challenge of isolating shear stress as a variable. This necessitates a more controlled environment using an *in vitro* model. We achieved this by applying varying magnitudes of shear stress on human monocyte-derived macrophages (MDMs) using a cone-and-plate viscometer and evaluating changes in morphology, gene expression, protein expression, and cytokine secretion over time. MDMs exposed to shear stress exhibited a rounder morphology compared to statically-cultured controls. RT-qPCR results showed significant upregulation of TNF-α, and analysis of cytokine release revealed increased secretion of TNF-α, IL-18, fractalkine, and other chemokines. The upregulation of pro-inflammatory factors was evident with both increasing magnitudes of shear and time. Taken together, these results indicate that prolonged shear exposure induced a pro-inflammatory M1 phenotype. These findings have implications for medical technology development, such as *in situ* vascular graft design wherein macrophages are exposed to shear and have been shown to affect graft resorption, and in delineating disease pathophysiology, for example to further illuminate the role of macrophages in atherosclerosis where shear is directly related to disease outcome.

1. Introduction

Macrophages are innate immune cells that are involved in wound healing, fighting infection, and stimulating other immune cells in response to injury. They readily adopt a wide spectrum of phenotypes regulated by the biochemical cues from their surrounding microenvironment, which enables these cells to play a critical role in wound healing regulation. Upon exposure to pro-inflammatory signals such as interferon-γ (IFN-γ) and lipopolysaccharide (LPS), macrophages classically activate into the pro-inflammatory M1 phenotype and genetically express markers such as tumor necrosis factor-α (TNF-α) and chemokine receptor CCR7 (1-3). M1 macrophages dominate the pro-inflammatory phase of wound healing, clearing cellular debris and secreting pro-inflammatory cytokines and chemokines, such as TNF-α, IL-1β, IL-6, IL-12, and IL-23 (4). By contrast, exposure to anti-inflammatory signals such as interleukin (IL)-4 and IL-13 incurs alternative activation into the anti-inflammatory M2 phenotype characterized by the expression of transforming growth factor-β (TGF-β) and mannose receptor MRC1 (1, 2). M2 macrophages are heavily involved in wound resolution and fibrosis and secrete factors such as IL-10 and TGF-β that dampen the inflammatory response (5). In addition to differences in gene and protein expression, M1 and M2 macrophages display distinct morphological variations. M1 macrophages exhibit the traditional "fried egg" morphology, whereas M2 macrophages are elongated and spindle-like (6, 7). Overall, it is accepted that biochemical signals induce complex responses from macrophages through changes in gene expression, protein secretion, and morphology.

While much of the current research has focused on the role of cytokines and chemokines in regulating macrophage plasticity, the role of the mechanical microenvironment has received considerably less attention. Macrophages respond to their surrounding mechanical microenvironment through a process called mechanotransduction. Through this process, they sense mechanical stimuli, such as stiffness and topography, which they convert into biochemical signals. Recent works have shown that the degree of stiffness regulates the differentiation and function of macrophages (8-10). Specifically, increased stiffness, as seen in fibrotic tissue, drives macrophage polarization towards an anti-inflammatory M2 phenotype (10). Accordingly, macrophages in fibrotic tissue exhibit an elongated morphology (6). Findings have also shown that macrophages can be induced to polarize by directly modulating their morphology. For example, McWhorter et al. engineered cell culture substrates to control macrophage morphology and concluded that elongating the macrophage morphology upregulated the expression of M2 markers and reduced the secretion of pro-inflammatory cytokines (6). Aside from stiffness and topology, macrophages can be influenced by dynamic mechanical loading, such as stretch and compression. Studies of human monocyte-derived macrophages (MDMs) have shown that cyclic stretch induces their expression of matrix metalloproteinase (MMP)-1 and MMP-3 and encourages their differentiation into osteoclasts for bone repair and maintenance (11, 12). Overall, these investigations demonstrate that macrophage morphology and behavior are not only influenced by cellular signals, but also by the mechanical forces imposed upon them.

Although researchers have begun to investigate the effect of various mechanical stimuli on macrophages, there is a paucity of research over their response to shear stress. Recent works

investigating macrophage behavior in shear stress conditions have primarily been focused on atherosclerotic plaque formation (4, 13, 14). Specifically, *in vivo* mouse models of atherosclerosis have shown that steady high shear within straight regions of coronary arteries is atheroprotective, dominated by macrophages expressing M2 markers, and correlated with plaque stability, whereas disturbed low shear at bifurcations is atheroprone, rich in M1 macrophages, and vulnerable to plaque rupture (13, 15, 16). However, there are other regions of the heart and cardiovascular system where the effects of high shear stresses are less clear. One example is the left ventricular outflow tract (LVOT), where high shear stresses are putatively associated with discrete subaortic stenosis (DSS), the formation of a membrane structure that encircles the LVOT and narrows the pathway to the aortic valve, increasing shear stress (17). Analysis of septal myectomy in patients with DSS has revealed glycosaminoglycan and proteoglycan deposition, along with evidence of inflammation, suggesting that macrophages may contribute to the development of this fibrous membrane (18, 19).

The specific role of shear stress in macrophage response, however, remains an open question. Although other studies have evaluated hemodynamic loading on macrophages in the context of biomaterial-driven *in situ* vascular regeneration and shown that macrophage activation is augmented upon exposure to shear stress (20-22), there is limited knowledge about the biomolecules that macrophages release in response to these changes. Furthermore, *in vivo* studies have difficulty teasing out the specific effects of fluid shear stress on macrophages considering that other factors such as stiffness and cellular signaling also influence macrophage function. Therefore, in this study, we employed an *in vitro* model system to characterize macrophage behavior under various rates of physiological shear (23, 24). Human MDMs were exposed to 15 dynes/cm^2 and 35 dynes/cm^2 shear stress over a period of 3, 24, and 48 hours using a cone-and-plate viscometer. The macrophages were then evaluated for morphology, gene expression, protein expression, and cytokine secretion, enabling the study of the direct effects of shear stress on macrophage behavior, which, in turn, can help better define the role of macrophages in cardiovascular diseases.

2. Materials and Methods

2.1 Primary human monocyte-derived macrophages

Human monocytes were isolated from donor buffy coats received from the Gulf Coast Regional Blood Center (Houston, TX). Use of de-identified blood product samples received through a third party were deemed by the Rice University IRB to not be human subjects' research. The buffy coats were layered on top of 15 mL of Histopaque (1.077 g/mL; Sigma-Aldrich) and centrifuged at 400 x g for 30 minutes at room temperature without brake. Following centrifugation, the peripheral blood mononuclear cells (PBMCs) were collected from the interphase, pooled together from 3-4 donors, and washed twice with 1x PBS containing 5 mM EDTA. PBMCs were seeded onto tissue-culture treated flasks in RPMI 1640 (Sigma-Aldrich) supplemented with 10% fetal bovine serum (FBS), 1% penicillin/streptomycin, and MCSF (20 ng/µL; Novus Biologicals). After 24 hours, the floating lymphocytes were aspirated, and the flask was washed 2x with PBS to remove remaining lymphocytes, leaving attached monocytes. Monocytes were cultured in a 5% CO_2 incubator at

37°C for a subsequent 5-7 days in RPMI 1640 supplemented with 10% FBS, 1% penicillin/streptomycin, and MCSF (20 ng/µL). Media was replenished on days 3 and 5. On days 5-7, macrophages were harvested after incubation with Accutase (Sigma-Aldrich) for 15 minutes along with gentle cell scraping.

2.2 Shear stress application

Uniform laminar shear stress was applied to primary human MDMs using a cone-and-plate viscometer system placed in a 5% CO_2 incubator at 37°C. The cone was placed on top of a 60 mm petri dish seeded with a monolayer of MDMs that was then positioned on top of a controllable magnetic stir plate. The static condition (0 RPM) did not have a cone placed on top of the petri dish. Each petri dish was washed with PBS and supplemented with 3 mL of fresh MDM media (RPMI 1640 supplemented with 10% FBS and 1% penicillin/streptomycin) prior to shear exposure. The cone was then rotated at 280 RPM or 660 RPM, which equated to a shear rate of 15 dynes/cm^2 and 35 dynes/cm^2, respectively, using the governing wall shear stress equation:

$$\tau = \mu\left(\frac{\omega \cdot r}{r \cdot \alpha + \chi}\right)$$

where τ is the desired shear stress, µ is the dynamic viscosity (0.95 centistokes) of the media, ω is the angular velocity of the cone, r is the radius (30 mm) of the cone, α is the angle (0.5°) of the cone, and χ is the gap height (300 µm) between the cone and the cells. MDMs were exposed to these shear rates for 3, 24, or 48 hours, and phenotypes were then evaluated through flow cytometry and RT-qPCR. The 48-hour 35 dynes/cm^2 group was supplemented with an extra 1 mL of RPMI 1640 without serum after 24 hours to prevent the samples from drying out during the duration of the experiment.

2.3 Flow cytometry

After isolation and differentiation, MDMs were evaluated for purity through flow cytometry for expression of the pan-macrophage marker, CD68. MDMs were harvested after 15 minutes of Accutase exposure through gentle scraping. For intracellular staining, MDMs were fixed with 4% paraformaldehyde for 20 minutes at 4°C, washed 2x with 1% FBS in PBS, and permeabilized in PBS with 0.5% Tween20 and 1% FBS for 15 minutes at room temperature. Cells were then washed 2x with 1% FBS in PBS and incubated in 1% FBS in PBS with APC-conjugated mouse anti-human CD68 (BD Biosciences) for 1 hour at room temperature. Following staining, samples were washed 2x with 1% FBS in PBS and transferred to 5 mL flow cytometry tubes.

Following shear stress application, the MDM protein expression of characteristic phenotypic markers was evaluated using flow cytometry. Cells were stained with the following antibodies: FITC-conjugated mouse anti-human CD80 (BD Biosciences), PE-conjugated mouse anti-human CD163 (BD Biosciences), and APC-conjugated mouse anti-human CD206 (BD Biosciences). Briefly, MDMs were harvested after 15 minutes of Accutase exposure through gentle scraping. Cells were incubated in 1% FBS in PBS with all antibodies for 30 minutes at room temperature. Non-specific binding was blocked by incubating the samples with 1% FBS in PBS. Following

staining, samples were washed 2x with 1% FBS in PBS and transferred to 5 mL flow cytometry tubes. Flow cytometry data for all markers was acquired using the Sony MA900 multi-application cell sorter (Sony Biotechnology Inc) and was analyzed using FlowJo.

2.4 Viability staining and morphology quantification

Cell viability was assessed following shear stress application by incubating each sample in a solution containing 2 μM calcein AM and 4 μM ethidium homodimer-1 in PBS (Live/Dead Viability/Cytotoxicity Kit; Thermo Fisher) for 30 minutes at room temperature. Samples were imaged immediately via fluorescent microscopy. Cell viability was quantified through FIJI. Morphology was analyzed using FIJI's circularity feature where circularity is defined as 4π*area/perimeter. A perfect circle has a circularity of 1. The circularity of each individual cell was analyzed from each group's live/dead images resulting in a large number of samples.

2.5 RNA isolation, cDNA synthesis, and quantitative reverse transcription PCR

Following shear stress application, MDM phenotypes were evaluated through quantitative reverse transcription PCR (RT-qPCR). RNA was extracted using the Direct-zol™ RNA Microprep kit (Zymo Research) according to the manufacturer's instructions. Briefly, MDMs were lysed with TRIzol (Thermo Fisher), mixed with an equal volume of 95% ethanol, and transferred to a Zymo-Spin™ IC Column in a collection tube. Samples were then incubated with DNase I for 15 minutes at room temperature, washed with RNA wash buffer, and eluted with 15 μL of DNase/RNase-free water. RNA purity ($A_{260/280}$ > 1.8) was then assessed through the NanoDrop 2000 spectrophotometer (Thermo Fisher), and RNA was stored at -80°C until further steps. Complementary DNA (cDNA) was synthesized from purified RNA using the High-Capacity cDNA Reverse Transcription Kit (Applied Biosystems) according to manufacturer's instructions and then stored at -20°C until gene expression analysis. RT-qPCR was performed using the iTaq™ Universal Probes Supermix (Bio-Rad Laboratories) according to manufacturer's instructions with primers specific to human CCR7 (probe ID: Hs01013469_m1), MRC1 (Hs02832368_g1), TGFB1 (Hs00998133_m1), TNF (Hs00174128_m1), and GAPDH (Hs02786624_g1) (Applied Biosystems). Fold changes were first normalized to GAPDH and then to the control group (no shear stress application).

2.6 Conditioned media analysis

After shear exposure, conditioned media containing cytokines secreted by MDMs were collected and centrifuged at 1000 x g for 5 minutes to remove cellular debris. The supernatant was then collected and stored at -80°C until cytokine analysis. Cytokines were analyzed using the MILLIPLEX® Human 48-Plex Cytokine Panel A kit (MilliporeSigma) on the Luminex system as per manufacturer's instructions. This analysis was done by the proteomics core laboratory at Baylor College of Medicine, Houston, TX. Briefly, samples were thawed on ice and centrifuged at 10000 x g for 5 mins. Samples and beads were incubated at 4°C on a shaker for 16 hours. Well contents were then removed, and the plate was washed 3x with 200 μL Wash Buffer. 25 μL of detection antibodies were added to each well and incubated at room temperature for 1 hour. 25 μL

of Streptavidin-Phycoerythrin was then added to each well containing the detection antibodies and incubated for 30 minutes at room temperature. Well contents were removed, and the plate was washed 3x with 200 µL Wash Buffer. 150 µL of Sheath Fluid PLUS was added to all wells, beads were resuspended on a plate shaker for 5 minutes, and the plate was read on the Luminex system. RPMI-1640 media was used as the blank. Two quality control samples were prepared, and a Logistic-5PL regression type was used to construct the standard curve of all the analytes.

2.7 Statistical analysis

Statistical analysis was performed using GraphPad Prism software version 6 (GraphPad Software Inc.) and R. A two-way analysis of variance (ANOVA) with post-hoc Tukey's testing was used to determine statistical significance ($p < 0.05$) for each set of conditions in this study. All experiments were repeated in triplicates.

3. Results

3.1 Shear stress exposure modulated MDM morphology by reducing elongation

A cone-and-plate viscometer was used to apply varying shear rates (0 dynes/cm^2 (static), 15 dynes/cm^2, and 35 dynes/cm^2) to MDMs for a period of 3, 24, and 48 hours (**Figure 1**). Post shear exposure, samples were treated with live/dead stain and imaged to evaluate cell viability (**Figure 2**). Additional bright-field images were taken to examine cell morphology (**Figure 3**). As shown in the fluorescent images, cell viability did not change over time or shear rate (93% average viability). Morphological changes were determined using the circularity measurement in FIJI; approximately 500 cells were measured across 4 dishes per condition. Interestingly, all groups were generally more elongated (less circular) as time increased (**Figure 3, Supplementary Figure 1**). Exposure to shear at each timepoint increased circularity, aside from the 48-hour timepoint where the 35 dynes/cm^2 condition was not significantly different than static. These results indicate that MDMs were expressing a rounder morphology in response to shear.

3.2 Shear stress attenuated MDM protein expression

MDM protein expression was also evaluated through flow cytometry after shear exposure (**Figure 4**). We investigated CD80 as a marker for M1 phenotype, and CD206 and CD163 as markers for M2 phenotype. CD80 surface marker expression was downregulated in response to increasing time in all groups. This downregulation was evident across all timepoints in response to increasing shear except for 48 hours where expression remained unchanged. Interestingly, CD163 expression generally remained unchanged in the static condition over time after an initial downregulation but exhibited attenuated expression levels in response to shear. Similarly, CD206 expression remained unaffected by time within the static and 15 dynes/cm^2 groups but was significantly downregulated at 48 hours in the 35 dynes/cm^2 group. Overall, prolonged exposure to shear stress reduced MDM protein expression.

3.3 Shear stress upregulated gene expression of TNF-α in a time-dependent manner

After shear exposure, RNA was isolated from samples, and RT-qPCR was performed to evaluate the effect of shear and the effect of time on MDM gene expression. We investigated TNF, which codes for TNF-α, and CCR7 as markers for inflammation and M1 phenotype; and TGF-β1 and MRC1, which codes for CD206, as markers for fibrosis and M2 phenotype. Looking within each shear condition, TNF was strongly upregulated at 24 hours in both shear conditions, while CCR7 remained relatively unaffected aside from the 15 dynes/cm^2 condition with downregulation at 48 hours. TGF-β1 was downregulated at 24 hours within the 35 dynes/cm^2 condition, while MRC1 was downregulated at both 24 and 48 hours in response to shear. Looking within each timepoint, there were no differences in gene expression among groups at 3 hours in response to increasing shear, whereas changes were seen at 24 and 48 hours. Specifically, the expression of TNF was most elevated at the 24-hour timepoint where increasing magnitudes of shear promoted significant upregulation compared to static controls (7.36 vs. 16.87-fold change for the two shear magnitudes, respectively, **Figure 5**). CCR7 expression demonstrated a downward trend starting at 24 hours with significant downregulation at 48 hours in response to increasing shear. Meanwhile, TGF-β1 was downregulated at 24 hours in the 35 dynes/cm^2 group, and MRC1 displayed no significant changes in expression levels. Overall, the prominent upregulation of TNF in response to shear within the 24 hour timepoint indicated that MDMs may be expressing an inflammatory phenotype upon exposure to shear.

3.4 Shear stress promoted time-dependent pro-inflammatory cytokine secretion

3.4.1 Cytokine secretion in response to time within each shear condition

Since gene expression of TNF-α was considerably upregulated compared to other markers, we analyzed conditioned media for cytokine levels using a 48-plex cytokine panel. The results shown in **Figures 6-8** demonstrate that both shear rate and time affected cellular signaling. Interestingly, within each shear condition, increasing time overwhelmingly correlated with monotonically increased production of chemokines and pro-inflammatory cytokines (**Figures 6-7**). IFN-γ, granulocyte-colony stimulating factor (G-CSF), and numerous chemokines (IL-8, IL-15, monocyte chemoattractant protein-1 (MCP-1), macrophage-derived chemokine (MDC), and chemokine ligand 9 (CXCL9)), were all increased in response to prolonged time across the different shear conditions. In contrast, the inflammatory chemokines, macrophage inflammatory protein (MIP)-1α and MIP-1β were both downregulated over time, but only in the static condition.

Secretion of the anti-inflammatory cytokines, however, was varied (**Figures 6&8**). Epidermal growth factor (EGF) production in the static condition was upregulated at 24 hours (vs. 3 hours) but was downregulated at 48 hours. Furthermore, it remained significantly downregulated in the 15 and 35 dynes/cm^2 conditions as time increased. Fibrotic growth factor-2 (FGF-2) remained generally unchanged over time but had decreased levels at 24 hours vs. 3 hours in the 15 dynes/cm^2 condition. IL-1RA was upregulated across all timepoints within the static and 15 dynes/cm^2 conditions but was downregulated at 48 hours in the 35 dynes/cm^2 condition. Vascular endothelial growth factor-A (VEGF-A) and platelet derived growth factor-AA (PDGF-AA) were upregulated in the 15 and 35 dynes/cm^2 conditions over time but remained unchanged in the static condition.

3.4.2 Cytokine secretion in response to increasing shear magnitude within each timepoint

Increasing shear, however, stimulated paradoxical effects within different timepoints. Among the pro-inflammatory cytokines (**Figures 6-7**), CXCL9 and TNF-α were downregulated in response to increasing shear at 3 hours. However, at 24 and 48 hours, these cytokines were upregulated following increased shear. Secretion of IFN-γ and IL-8 was unaffected at 3 hours but was significantly upregulated in response to shear at 24 hours. MCP-3 secretion was unaffected by shear at 3 hours but was upregulated at 24 and 48 hours in response to 35 dynes/cm^2 of shear. MCP-1 secretion initially decreased at 3 hours in response to increasing shear but remained unaffected at 24 and 48 hours. RANTES was not affected by increased shear at 3 and 48 hours but was significantly upregulated in response to 35 dynes/cm^2 of shear at 24 hours. MIP-1α and MIP-1β were significantly downregulated at 3 hours with increasing shear but were unaffected at 24 and 48 hours. Eotaxin and fractalkine/CX_3CL1, potent chemoattractants for eosinophils and monocytes/T cells, respectively, showed more secretion with increased shear at every timepoint. However, this result was most significant at the 3-hour and 48-hour timepoints. Interestingly, fractalkine was not found in the static conditioned media at any timepoint.

Looking at the effects of increased shear on anti-inflammatory cytokine release within each timepoint (**Figures 6&8**), EGF was upregulated in response to increased shear at 3 hours. However, the 24-hour timepoint showed the opposite pattern with less EGF secretion in response to increased shear. IL-10, a major cytokine secreted by M2 macrophages, was profoundly downregulated following increased shear at 3 hours, and maintained low abundance for all shear conditions at the 24- and 48-hour timepoints. PDGF-AA and VEGF-A secretions were unchanged by shear at the 3-hour timepoint but were monotonically upregulated by increasing shear at both the 24- and 48-hour timepoints. IL-1RA secretion was unchanged by shear at the 3- and 24-hour timepoints but was upregulated at 48 hours in the 15 dynes/cm^2 condition. Overall, the cytokine panel revealed a predominantly pro-inflammatory response towards prolonged shear exposure.

4. Discussion

Macrophages are highly plastic cells that polarize to M1 or M2 phenotypes in response to changes in their microenvironment, which enables them to play crucial roles in the wound healing process; correspondingly, they are heavily involved in major disease outcomes (19, 25-27). A surplus of one phenotype over the other has been shown to induce and promote pathological disease states. For example, chronic inflammatory diseases are associated with an overabundance of M1 macrophages (28, 29). In contrast to M1 overabundance, excessive quantities of M2 macrophages can result in pathological cardiac fibrosis and organ failure (30, 31). Therefore, a delicate balance between the M1 and M2 populations is necessary to maintain homeostasis. One stimulus that regulates this phenotypic balance is the mechanical microenvironment (32). For example, macrophages exposed to moderate magnitudes of cyclic strain (7%) have been shown to increase the ratio of M2/M1 macrophages, while high magnitudes of strain (12%) reduced this ratio (33). Although recent investigations have focused on the response of macrophages to the mechanical aspects of their environment, there is limited research surrounding macrophage behavior under shear stress. *In vivo* models of atherosclerosis have shown that macrophage phenotype, which is

vital in determining plaque rupture, is regulated by shear stress (13, 15). *In vitro* studies of macrophages have shown shear-dependent changes in morphology and von Willebrand factor uptake (34, 35). Additionally, Wissing et al. revealed that macrophage-induced vascular graft degradation is influenced by shear stress (21, 22). Although these works demonstrate that shear stress influences macrophage phenotype and behavior, it is difficult to evaluate the specific factors involved. In the present study, we subjected human MDMs to physiological levels of shear using a cone-and-plate viscometer over the course of 3, 24, and 48 hours. Our main findings were that MDMs expressed time-dependent changes in pro-inflammatory cytokine secretion, gene expression, and morphology in response to shear stress. Specifically, initial exposure to shear stress downregulated pro-inflammatory cytokine secretion at 3 hours, but an opposite effect was observed after prolonged shear at 24 and 48 hours. This phenotypic switch was also consistent when looking at gene expression, where TNF was upregulated while pro-fibrotic genes were downregulated at 24 hours.

The application of shear stress, over time, largely induced pro-inflammatory cytokine secretion by human MDMs. This finding was demonstrated by noting that levels of TNF-α and IFN-γ, potent activators of M1 macrophages, G-CSF, a neutrophil regulator, and numerous chemokines (IL-8, IL-15, MCP-1, MCP-3, MDC, RANTES, and CXCL9), significantly increased in response to prolonged shear exposure. These chemokines potently attract a wide variety of leukocytes including neutrophils, T-cells, monocytes, and macrophages (36-41). To further support MDM chemotactic response following shear exposure, eotaxin and fractalkine, potent chemoattractants for eosinophils and monocytes/T cells, were upregulated in response to shear at every timepoint (42, 43). Notably, fractalkine was not expressed in the static condition at any timepoint, indicating that shear stress exposure definitively induces macrophage-derived fractalkine secretion. Interestingly, protein levels for chemokines MIP-1α and MIP-1β were significantly downregulated in response to increased time in the static condition and exhibited the same trend following exposure to 15 dynes/cm^2 of shear. The conflicting results between chemokine expressions over time could be the result of different mechanisms of regulation. The mechanisms promoting MIP-1α expression in macrophages are not well understood, although the TLR4-IRF3 pathway is reported to be involved (44). Furthermore, MIP-1α release by macrophages is reported to be downregulated by IFN-γ *in vitro*, which is consistent with our results (45). IL-15, however, has been shown to induce IL-8 and MCP-1 production which may further promote leukocyte chemotaxis (46). Overall, the overwhelming upregulation of chemokines suggests that macrophages are becoming more pro-inflammatory and releasing signals to attract other leukocytes under prolonged exposure to shear stress.

In comparison to pro-inflammatory cytokines, levels of anti-inflammatory/pro-fibrotic cytokines secretion was diverse after shear exposure. IL-10, which is distinctly produced by M2 macrophages, was heavily suppressed with increasing shear. Furthermore, the downregulation of EGF in the 35 dynes/cm^2 condition at 24 and 48 hours was consistent with the upregulation of pro-inflammatory cytokine production with prolonged shear. To expand on this point, the secretion of pro-inflammatory cytokines MCP-3 and RANTES initially remained unchanged at the 3-hour

timepoint but experienced subsequent monotonic upregulation at later timepoints. Similarly, CXCL9, TNF-α, IFN-γ, IL-8, MCP-1, and MDC were initially downregulated at 3 hours in response to increasing shear but also experienced monotonic upregulation at subsequent timepoints. EGF exhibited an opposite trend compared to these cytokines with initial upregulation at 3 hours in response to increasing magnitudes of shear and subsequent downregulation at later timepoints, suggesting that EGF may play a role in regulating downstream pro-inflammatory macrophage response. Furthermore, aside from promoting cell proliferation and invasion (47), EGF has also been shown to induce monocyte chemotaxis (48). Interestingly, VEGF-A and PDGF-AA had higher levels of expression over longer time points in both shear conditions. Both of these growth factors are heavily regulated by M2 macrophages and involved in cell differentiation, proliferation, and angiogenesis. However, VEGF-A has also been reported to stimulate monocyte/macrophage chemotaxis (49). Furthermore, studies have also shown that M1 macrophages secrete the highest levels of VEGF-A compared to other macrophage phenotypes, and that IL-10 suppresses M1 but not M2-derived VEGF, which is consistent with our data (3, 50). These results suggest that VEGF-A plays a pro-inflammatory role in response to shear stress. Taken together, although these cytokines are generally considered anti-inflammatory/pro-fibrotic, they may be contributing to an overall pro-inflammatory response.

Evaluation of gene expression and morphology further supports that MDMs express a pro-inflammatory phenotype after shear exposure. The predominant findings were that CCR7 and MRC1, respective M1 and M2 markers, were significantly downregulated in response to prolonged shear. The downregulation of CCR7 was unexpected, but it would be worth investigating other gene markers for M1 macrophages such as CXCL10 and CXCL11. However, TNF, a prominent M1 marker, was significantly upregulated at 24 hours by a large magnitude while TGF-β1, an M2 marker, was downregulated at 24 hours as shear increased. Although MDMs were more elongated in response to time, the application of shear curbed their elongation and promoted maintenance of a round morphology. Interestingly, although there was a shift in MDM morphology indicative of a phenotypic switch, protein expression for both phenotypes were attenuated with shear exposure. The downregulation of CD80 expression over time in the static condition matches the morphology results, indicating that MDMs are becoming more M2-like over time. We believe that MDMs may be activated from initial seeding and adjusting to their environment. However, we expected the application of shear stress to promote CD80 expression. This attenuation could be due to macrophages expressing other M1 polarization markers that were not investigated such as CD86. Overall, our morphological evaluation coupled with the RT-qPCR results indicated that the MDMs may be primed towards a pro-inflammatory phenotype following shear exposure.

To our knowledge, this is the first study to characterize MDM phenotype in response to shear stress *in vitro*. While our results demonstrating the effect of shear stress on MDMs are very compelling, they must be considered in context. Although donors were kept consistent for RT-qPCR and Luminex analysis, a different set of donors was required for the flow cytometry analysis due to cell shortage. This could possibly account for the conflicting results between these data. Furthermore, it is difficult to test longer timepoints with this model without media replenishment

given that media evaporation will occur at longer timepoints. Although cells were seeded at a consistent density, cell detachment after shear exposure was not uncommon and could contribute to varying expression levels. Nonetheless, the results of gene expression, protein secretion, and morphology all demonstrate that exposure to shear stress drives a pro-inflammatory response from human MDMs, which is consistent with previous similar works (13, 51, 52). Fahy et al. exposed monocytes to shear and dynamic compression and observed an increase in TNF-α protein secretion and IL-8 gene expression (51). An *ex vivo* femoral artery model showed significant upregulation of pro-inflammatory cytokines TNF-α and MCP-1 in response to altered wall shear stress. Furthermore, previous *in vivo* studies have shown that low shear induces an M1 phenotype in atherosclerotic plaques (13, 15).

The results from our studies have implications for the role of MDMs in diseases involving altered shear stresses, such as atherosclerosis and DSS. Studies have shown that M1 macrophages are prominent in atheroprone regions, and M2 macrophages are dominant in stable plaques (13, 15, 16). The stark dichotomy between pro-inflammatory cytokine expression at the 3-hour timepoint compared to EGF is worth investigating in this context. These cytokines have all been implicated in the initiation and progression of atherosclerotic plaques. In atherosclerosis, fractalkine is present in low shear atheroprone regions, and its inhibition reduced leukocyte adhesion to inflamed endothelial cells (53, 54). The interaction between RANTES and fractalkine is established as an early pathway for rolling monocytes to firmly adhere to activated endothelium, and MCP-1 enables transendothelial migration (55). IL-8 assists with the firm adherence of monocytes to endothelium but is also implicated in potentiating plaque angiogenesis with its elevated presence in late-stage lesions (55). Furthermore, CXCL9 is known to promote differentiation and multiplication of leukocytes, cause tissue extravasation, and is upregulated in atherosclerosis (36, 56). Studies have also shown that the inhibition of TNF-α and IFN-γ have reduced atherosclerotic lesion size and regressed plaque progression (57, 58). Interestingly, inhibition of EGFR has been demonstrated to attenuate atherosclerosis by decreasing pro-inflammatory cytokines, such as TNF-α and IL-6 (59, 60). Given that our results show an initial increase in EGF secretion followed by subsequent downregulation, an interesting question postulates whether shear stress enhances the activity of EGFR, promoting the downstream pro-inflammatory response. One study observed an increase in EGFR expression and activation in response to fluid flow in a 3D ovarian cancer model (61). Interestingly, mutant EGFR, along with Ptpn11, which encodes for protein-tyrosine-phosphatase Shp2, has also been implicated in the development of defective semilunar cardiac valves causing enlargement from an overabundance of mesenchymal cells (62-64). Specifically, activation of the MAPK pathway through EGFR has been proven to drive epithelial–mesenchymal transition (EMT) in semilunar valve formation (64, 65). In the context of DSS, where altered shear and circulating immune cells are hypothesized to play a role in subvalvular fibrosis (17), it would be interesting to investigate the interactions between MDMs, shear stress, and EGFR.

The results from our studies should also be considered when designing *in situ* vascular grafts. Acellular vascular implants have been a promising approach for replacing small-diameter arteries. These biodegradable scaffolds promote new tissue formation, cellular infiltration, and ECM

deposition (66). However, the rate of scaffold degradation heavily influences patient outcomes. If the degradation is too quick, insufficient repair and loss of structural integrity occurs (67). In contrast, slow degradation could cause chronic inflammation and subsequent fibrosis (67). Macrophages have been demonstrated to affect the rate of scaffold degradation given their secretion of cytokines promoting both inflammation and wound resolution (22, 68). Consequently, the design of scaffolds that modulate the balance between M1/M2 phenotypes has been a promising approach. Given that these scaffolds are exposed to shear stress after implantation, Wissing et al. investigated the effect of these hemodynamic loads on macrophage-induced scaffold degradation (22). The authors revealed that shear stress enhanced THP-1 macrophage activation in biomaterial scaffolds by upregulating both pro-inflammatory and anti-inflammatory cytokines (22). Interestingly, CCR7 gene expression was downregulated in response to shear, consistent with our results. Furthermore, conditioned media from these macrophages upregulated genes involved in tissue formation and remodeling in fibroblasts. Since THP-1 macrophages have a different secretory profile than MDMs, it would be interesting to repeat these studies using MDMs due to their physiological relevance.

In conclusion, in the present study, we sought to investigate macrophage response to shear stress by characterizing human MDM gene expression, protein expression, and cytokine secretion after shear exposure. We have demonstrated that prolonged shear exposure induces a pro-inflammatory response from MDMs through the upregulation of pro-inflammatory cytokine secretion, gene expression, and change in morphology. The results of this work suggest that macrophages directly contribute to atherosclerotic plaque outcome and should be considered when designing *in situ* vascular grafts where MDMs are exposed to hemodynamic shear stress which can affect the rate of graft resorption and tissue promotion. Future work should investigate longer timepoints since fibrosis is the product of most chronic inflammatory diseases (69).

5. Acknowledgements

Financial support for this research was provided by a gift from Lew and Laura Moorman, NIH R01 HL140305 (to J-GA and SK), and NSF Graduate Research Fellowship Program (to EJ).

6. Author Contributions

Conceptualization: EJ, JC, SK, and JG-A. Investigation: EJ, GK, and HP. Formal analysis: EJ. Writing – original draft: EJ. Writing – review & editing: EJ, GK, KS, JP, and JG-A. Methodology: EJ, GK, KS, JP, and JG-A. Supervision: RB, JP, SK, and JG-A. Funding acquisition: SK and JG-A. All authors contributed to the article and approved the final submitted version.

References

1. Orecchioni M, Ghosheh Y, Pramod AB, Ley K. Macrophage Polarization: Different Gene Signatures in M1(Lps+) Vs. Classically and M2(Lps-) Vs. Alternatively Activated Macrophages. *Front Immunol* (2019) 10:1084. Epub 2019/06/11. doi: 10.3389/fimmu.2019.01084.
2. Smith TD, Tse MJ, Read EL, Liu WF. Regulation of Macrophage Polarization and Plasticity by Complex Activation Signals. *Integr Biol (Camb)* (2016) 8(9):946-55. Epub 2016/08/06. doi: 10.1039/c6ib00105j.
3. Spiller KL, Anfang RR, Spiller KJ, Ng J, Nakazawa KR, Daulton JW, et al. The Role of Macrophage Phenotype in Vascularization of Tissue Engineering Scaffolds. *Biomaterials* (2014) 35(15):4477-88. Epub 2014/03/05. doi: 10.1016/j.biomaterials.2014.02.012.
4. Lin P, Ji HH, Li YJ, Guo SD. Macrophage Plasticity and Atherosclerosis Therapy. *Front Mol Biosci* (2021) 8:679797. Epub 2021/05/25. doi: 10.3389/fmolb.2021.679797.
5. Lutgens E, Gijbels M, Smook M, Heeringa P, Gotwals P, Koteliansky VE, et al. Transforming Growth Factor-Beta Mediates Balance between Inflammation and Fibrosis During Plaque Progression. *Arterioscler Thromb Vasc Biol* (2002) 22(6):975-82. Epub 2002/06/18. doi: 10.1161/01.atv.0000019729.39500.2f.
6. McWhorter FY, Wang T, Nguyen P, Chung T, Liu WF. Modulation of Macrophage Phenotype by Cell Shape. *Proc Natl Acad Sci U S A* (2013) 110(43):17253-8. Epub 2013/10/09. doi: 10.1073/pnas.1308887110.
7. Heinrich F, Lehmbecker A, Raddatz BB, Kegler K, Tipold A, Stein VM, et al. Morphologic, Phenotypic, and Transcriptomic Characterization of Classically and Alternatively Activated Canine Blood-Derived Macrophages in Vitro. *PLoS One* (2017) 12(8):e0183572. Epub 2017/08/18. doi: 10.1371/journal.pone.0183572.
8. Gruber EJ, Leifer CA. Molecular Regulation of Tlr Signaling in Health and Disease: Mechano-Regulation of Macrophages and Tlr Signaling. *Innate Immun* (2020) 26(1):15-25. Epub 2020/01/21. doi: 10.1177/1753425919838322.
9. Gruber E, Heyward C, Cameron J, Leifer C. Toll-Like Receptor Signaling in Macrophages Is Regulated by Extracellular Substrate Stiffness and Rho-Associated Coiled-Coil Kinase (Rock1/2). *Int Immunol* (2018) 30(6):267-78. Epub 2018/05/26. doi: 10.1093/intimm/dxy027.
10. Friedemann M, Kalbitzer L, Franz S, Moeller S, Schnabelrauch M, Simon JC, et al. Instructing Human Macrophage Polarization by Stiffness and Glycosaminoglycan Functionalization in 3d Collagen Networks. *Adv Healthc Mater* (2017) 6(7). Epub 2017/01/31. doi: 10.1002/adhm.201600967.
11. Yang JH, Sakamoto H, Xu EC, Lee RT. Biomechanical Regulation of Human Monocyte/Macrophage Molecular Function. *Am J Pathol* (2000) 156(5):1797-804. Epub 2000/05/04. doi: 10.1016/S0002-9440(10)65051-1.
12. Maruyama K, Nemoto E, Yamada S. Mechanical Regulation of Macrophage Function - Cyclic Tensile Force Inhibits Nlrp3 Inflammasome-Dependent Il-1beta Secretion in Murine Macrophages. *Inflamm Regen* (2019) 39:3. Epub 2019/02/19. doi: 10.1186/s41232-019-0092-2.
13. Seneviratne AN, Cole JE, Goddard ME, Park I, Mohri Z, Sansom S, et al. Low Shear Stress Induces M1 Macrophage Polarization in Murine Thin-Cap Atherosclerotic Plaques. *J Mol Cell Cardiol* (2015) 89(Pt B):168-72. Epub 2015/11/03. doi: 10.1016/j.yjmcc.2015.10.034.
14. De Wilde D, Trachet B, De Meyer GRY, Segers P. Shear Stress Metrics and Their Relation to Atherosclerosis: An in Vivo Follow-up Study in Atherosclerotic Mice. *Ann Biomed Eng* (2016) 44(8):2327-38. Epub 2015/12/24. doi: 10.1007/s10439-015-1540-z.

15. Seneviratne A, Hulsmans M, Holvoet P, Monaco C. Biomechanical Factors and Macrophages in Plaque Stability. *Cardiovasc Res* (2013) 99(2):284-93. Epub 2013/05/21. doi: 10.1093/cvr/cvt097.
16. Heo KS, Fujiwara K, Abe J. Shear Stress and Atherosclerosis. *Mol Cells* (2014) 37(6):435-40. Epub 2014/05/02. doi: 10.14348/molcells.2014.0078.
17. Masse DD, Shar JA, Brown KN, Keswani SG, Grande-Allen KJ, Sucosky P. Discrete Subaortic Stenosis: Perspective Roadmap to a Complex Disease. *Front Cardiovasc Med* (2018) 5:122. Epub 2018/10/16. doi: 10.3389/fcvm.2018.00122.
18. Butany J, Vaideeswar P, David TE. Discrete Subaortic Membranes in Adults--a Clinicopathological Analysis. *Cardiovasc Pathol* (2009) 18(4):236-42. Epub 2008/10/01. doi: 10.1016/j.carpath.2008.06.013.
19. Jui E, Singampalli KL, Shani K, Ning Y, Connell JP, Birla RK, et al. The Immune and Inflammatory Basis of Acquired Pediatric Cardiac Disease. *Front Cardiovasc Med* (2021) 8:701224. Epub 2021/08/14. doi: 10.3389/fcvm.2021.701224.
20. Smits AI, Ballotta V, Driessen-Mol A, Bouten CV, Baaijens FP. Shear Flow Affects Selective Monocyte Recruitment into Mcp-1-Loaded Scaffolds. *J Cell Mol Med* (2014) 18(11):2176-88. Epub 2014/08/12. doi: 10.1111/jcmm.12330.
21. van Haaften EE, Wissing TB, Kurniawan NA, Smits A, Bouten CVC. Human in Vitro Model Mimicking Material-Driven Vascular Regeneration Reveals How Cyclic Stretch and Shear Stress Differentially Modulate Inflammation and Matrix Deposition. *Adv Biosyst* (2020) 4(6):e1900249. Epub 2020/05/12. doi: 10.1002/adbi.201900249.
22. Wissing TB, van Haaften EE, Koch SE, Ippel BD, Kurniawan NA, Bouten CVC, et al. Hemodynamic Loads Distinctively Impact the Secretory Profile of Biomaterial-Activated Macrophages - Implications for in Situ Vascular Tissue Engineering. *Biomater Sci* (2019) 8(1):132-47. Epub 2019/11/12. doi: 10.1039/c9bm01005j.
23. Barral M, El-Sanharawi I, Dohan A, Sebuhyan M, Guedon A, Delarue A, et al. Blood Flow and Shear Stress Allow Monitoring of Progression and Prognosis of Tumor Diseases. *Front Physiol* (2021) 12:693052. Epub 2021/08/21. doi: 10.3389/fphys.2021.693052.
24. Samady H, Eshtehardi P, McDaniel MC, Suo J, Dhawan SS, Maynard C, et al. Coronary Artery Wall Shear Stress Is Associated with Progression and Transformation of Atherosclerotic Plaque and Arterial Remodeling in Patients with Coronary Artery Disease. *Circulation* (2011) 124(7):779-88. Epub 2011/07/27. doi: 10.1161/CIRCULATIONAHA.111.021824.
25. Zhang C, Yang M, Ericsson AC. Function of Macrophages in Disease: Current Understanding on Molecular Mechanisms. *Front Immunol* (2021) 12:620510. Epub 2021/03/26. doi: 10.3389/fimmu.2021.620510.
26. Ardura JA, Rackov G, Izquierdo E, Alonso V, Gortazar AR, Escribese MM. Targeting Macrophages: Friends or Foes in Disease? *Front Pharmacol* (2019) 10:1255. Epub 2019/11/12. doi: 10.3389/fphar.2019.01255.
27. Singampalli KL, Jui E, Shani K, Ning Y, Connell JP, Birla RK, et al. Congenital Heart Disease: An Immunological Perspective. *Front Cardiovasc Med* (2021) 8:701375. Epub 2021/08/27. doi: 10.3389/fcvm.2021.701375.
28. Parisi L, Gini E, Baci D, Tremolati M, Fanuli M, Bassani B, et al. Macrophage Polarization in Chronic Inflammatory Diseases: Killers or Builders? *J Immunol Res* (2018) 2018:8917804. Epub 2018/03/07. doi: 10.1155/2018/8917804.

29. Espinoza-Jimenez A, Peon AN, Terrazas LI. Alternatively Activated Macrophages in Types 1 and 2 Diabetes. *Mediators Inflamm* (2012) 2012:815953. Epub 2013/01/18. doi: 10.1155/2012/815953.
30. Wynn TA, Vannella KM. Macrophages in Tissue Repair, Regeneration, and Fibrosis. *Immunity* (2016) 44(3):450-62. Epub 2016/03/18. doi: 10.1016/j.immuni.2016.02.015.
31. Hulsmans M, Sam F, Nahrendorf M. Monocyte and Macrophage Contributions to Cardiac Remodeling. *J Mol Cell Cardiol* (2016) 93:149-55. Epub 2015/11/26. doi: 10.1016/j.yjmcc.2015.11.015.
32. McWhorter FY, Davis CT, Liu WF. Physical and Mechanical Regulation of Macrophage Phenotype and Function. *Cell Mol Life Sci* (2015) 72(7):1303-16. Epub 2014/12/17. doi: 10.1007/s00018-014-1796-8.
33. Ballotta V, Driessen-Mol A, Bouten CV, Baaijens FP. Strain-Dependent Modulation of Macrophage Polarization within Scaffolds. *Biomaterials* (2014) 35(18):4919-28. Epub 2014/03/26. doi: 10.1016/j.biomaterials.2014.03.002.
34. Castro-Nunez L, Dienava-Verdoold I, Herczenik E, Mertens K, Meijer AB. Shear Stress Is Required for the Endocytic Uptake of the Factor Viii-Von Willebrand Factor Complex by Macrophages. *J Thromb Haemost* (2012) 10(9):1929-37. Epub 2012/07/21. doi: 10.1111/j.1538-7836.2012.04860.x.
35. Rosenson-Schloss RS, Vitolo JL, Moghe PV. Flow-Mediated Cell Stress Induction in Adherent Leukocytes Is Accompanied by Modulation of Morphology and Phagocytic Function. *Med Biol Eng Comput* (1999) 37(2):257-63. Epub 1999/07/09. doi: 10.1007/BF02513296.
36. Tokunaga R, Zhang W, Naseem M, Puccini A, Berger MD, Soni S, et al. Cxcl9, Cxcl10, Cxcl11/Cxcr3 Axis for Immune Activation - a Target for Novel Cancer Therapy. *Cancer Treat Rev* (2018) 63:40-7. Epub 2017/12/06. doi: 10.1016/j.ctrv.2017.11.007.
37. Bickel M. The Role of Interleukin-8 in Inflammation and Mechanisms of Regulation. *J Periodontol* (1993) 64(5 Suppl):456-60. Epub 1993/05/01.
38. Szentes V, Gazdag M, Szokodi I, Dezsi CA. The Role of Cxcr3 and Associated Chemokines in the Development of Atherosclerosis and During Myocardial Infarction. *Front Immunol* (2018) 9:1932. Epub 2018/09/14. doi: 10.3389/fimmu.2018.01932.
39. Singh S, Anshita D, Ravichandiran V. Mcp-1: Function, Regulation, and Involvement in Disease. *Int Immunopharmacol* (2021) 101(Pt B):107598. Epub 2021/07/09. doi: 10.1016/j.intimp.2021.107598.
40. Opdenakker G, Froyen G, Fiten P, Proost P, Van Damme J. Human Monocyte Chemotactic Protein-3 (Mcp-3): Molecular Cloning of the Cdna and Comparison with Other Chemokines. *Biochem Biophys Res Commun* (1993) 191(2):535-42. Epub 1993/03/15. doi: 10.1006/bbrc.1993.1251.
41. Mikolajczyk TP, Nosalski R, Szczepaniak P, Budzyn K, Osmenda G, Skiba D, et al. Role of Chemokine Rantes in the Regulation of Perivascular Inflammation, T-Cell Accumulation, and Vascular Dysfunction in Hypertension. *FASEB J* (2016) 30(5):1987-99. Epub 2016/02/14. doi: 10.1096/fj.201500088R.
42. Mattes J, Foster PS. Regulation of Eosinophil Migration and Th2 Cell Function by Il-5 and Eotaxin. *Curr Drug Targets Inflamm Allergy* (2003) 2(2):169-74. Epub 2003/10/17. doi: 10.2174/1568010033484214.
43. White GE, Greaves DR. Fractalkine: A Survivor's Guide: Chemokines as Antiapoptotic Mediators. *Arterioscler Thromb Vasc Biol* (2012) 32(3):589-94. Epub 2012/01/17. doi: 10.1161/ATVBAHA.111.237412.

44. Sindhu S, Akhter N, Wilson A, Thomas R, Arefanian H, Al Madhoun A, et al. Mip-1alpha Expression Induced by Co-Stimulation of Human Monocytic Cells with Palmitate and Tnf-Alpha Involves the Tlr4-Irf3 Pathway and Is Amplified by Oxidative Stress. *Cells* (2020) 9(8). Epub 2020/08/06. doi: 10.3390/cells9081799.
45. Sherry B, Espinoza M, Manogue KR, Cerami A. Induction of the Chemokine Beta Peptides, Mip-1 Alpha and Mip-1 Beta, by Lipopolysaccharide Is Differentially Regulated by Immunomodulatory Cytokines Gamma-Ifn, Il-10, Il-4, and Tgf-Beta. *Mol Med* (1998) 4(10):648-57. Epub 1998/12/16.
46. Badolato R, Ponzi AN, Millesimo M, Notarangelo LD, Musso T. Interleukin-15 (Il-15) Induces Il-8 and Monocyte Chemotactic Protein 1 Production in Human Monocytes. *Blood* (1997) 90(7):2804-9. Epub 1997/11/05.
47. Haque A, Moriyama M, Kubota K, Ishiguro N, Sakamoto M, Chinju A, et al. Cd206(+) Tumor-Associated Macrophages Promote Proliferation and Invasion in Oral Squamous Cell Carcinoma Via Egf Production. *Sci Rep* (2019) 9(1):14611. Epub 2019/10/12. doi: 10.1038/s41598-019-51149-1.
48. Lamb DJ, Modjtahedi H, Plant NJ, Ferns GA. Egf Mediates Monocyte Chemotaxis and Macrophage Proliferation and Egf Receptor Is Expressed in Atherosclerotic Plaques. *Atherosclerosis* (2004) 176(1):21-6. Epub 2004/08/13. doi: 10.1016/j.atherosclerosis.2004.04.012.
49. Krettek A, Ostergren-Lunden G, Fager G, Rosmond C, Bondjers G, Lustig F. Expression of Pdgf Receptors and Ligand-Induced Migration of Partially Differentiated Human Monocyte-Derived Macrophages. Influence of Ifn-Gamma and Tgf-Beta. *Atherosclerosis* (2001) 156(2):267-75. Epub 2001/06/08. doi: 10.1016/s0021-9150(00)00644-4.
50. Wu WK, Llewellyn OP, Bates DO, Nicholson LB, Dick AD. Il-10 Regulation of Macrophage Vegf Production Is Dependent on Macrophage Polarisation and Hypoxia. *Immunobiology* (2010) 215(9-10):796-803. Epub 2010/08/10. doi: 10.1016/j.imbio.2010.05.025.
51. Fahy N, Menzel U, Alini M, Stoddart MJ. Shear and Dynamic Compression Modulates the Inflammatory Phenotype of Human Monocytes in Vitro. *Front Immunol* (2019) 10:383. Epub 2019/03/21. doi: 10.3389/fimmu.2019.00383.
52. Kadam AA, Gersch RP, Rosengart TK, Frame MD. Inflammatory Monocyte Response Due to Altered Wall Shear Stress in an Isolated Femoral Artery Model. *J Biol Methods* (2019) 6(1):e109. Epub 2019/08/28. doi: 10.14440/jbm.2019.274.
53. Zernecke A, Shagdarsuren E, Weber C. Chemokines in Atherosclerosis: An Update. *Arterioscler Thromb Vasc Biol* (2008) 28(11):1897-908. Epub 2008/06/21. doi: 10.1161/ATVBAHA.107.161174.
54. Cheng C, Tempel D, van Haperen R, de Boer HC, Segers D, Huisman M, et al. Shear Stress-Induced Changes in Atherosclerotic Plaque Composition Are Modulated by Chemokines. *J Clin Invest* (2007) 117(3):616-26. Epub 2007/02/17. doi: 10.1172/JCI28180.
55. Apostolakis S, Vogiatzi K, Amanatidou V, Spandidos DA. Interleukin 8 and Cardiovascular Disease. *Cardiovasc Res* (2009) 84(3):353-60. Epub 2009/07/21. doi: 10.1093/cvr/cvp241.
56. Zernecke A, Weber C. Chemokines in the Vascular Inflammatory Response of Atherosclerosis. *Cardiovasc Res* (2010) 86(2):192-201. Epub 2009/12/17. doi: 10.1093/cvr/cvp391.

57. Voloshyna I, Littlefield MJ, Reiss AB. Atherosclerosis and Interferon-Gamma: New Insights and Therapeutic Targets. *Trends Cardiovasc Med* (2014) 24(1):45-51. Epub 2013/08/07. doi: 10.1016/j.tcm.2013.06.003.
58. Branen L, Hovgaard L, Nitulescu M, Bengtsson E, Nilsson J, Jovinge S. Inhibition of Tumor Necrosis Factor-Alpha Reduces Atherosclerosis in Apolipoprotein E Knockout Mice. *Arterioscler Thromb Vasc Biol* (2004) 24(11):2137-42. Epub 2004/09/04. doi: 10.1161/01.ATV.0000143933.20616.1b.
59. Wang L, Huang Z, Huang W, Chen X, Shan P, Zhong P, et al. Inhibition of Epidermal Growth Factor Receptor Attenuates Atherosclerosis Via Decreasing Inflammation and Oxidative Stress. *Sci Rep* (2017) 8:45917. Epub 2017/04/05. doi: 10.1038/srep45917.
60. Zeboudj L, Giraud A, Guyonnet L, Zhang Y, Laurans L, Esposito B, et al. Selective Egfr (Epidermal Growth Factor Receptor) Deletion in Myeloid Cells Limits Atherosclerosis-Brief Report. *Arterioscler Thromb Vasc Biol* (2018) 38(1):114-9. Epub 2017/12/02. doi: 10.1161/ATVBAHA.117.309927.
61. Nath S, Pigula M, Khan AP, Hanna W, Ruhi MK, Dehkordy FM, et al. Flow-Induced Shear Stress Confers Resistance to Carboplatin in an Adherent Three-Dimensional Model for Ovarian Cancer: A Role for Egfr-Targeted Photoimmunotherapy Informed by Physical Stress. *J Clin Med* (2020) 9(4). Epub 2020/04/02. doi: 10.3390/jcm9040924.
62. Chen B, Bronson RT, Klaman LD, Hampton TG, Wang JF, Green PJ, et al. Mice Mutant for Egfr and Shp2 Have Defective Cardiac Semilunar Valvulogenesis. *Nat Genet* (2000) 24(3):296-9. Epub 2000/03/04. doi: 10.1038/73528.
63. Barrick CJ, Roberts RB, Rojas M, Rajamannan NM, Suitt CB, O'Brien KD, et al. Reduced Egfr Causes Abnormal Valvular Differentiation Leading to Calcific Aortic Stenosis and Left Ventricular Hypertrophy in C57bl/6j but Not 129s1/Svimj Mice. *Am J Physiol Heart Circ Physiol* (2009) 297(1):H65-75. Epub 2009/05/19. doi: 10.1152/ajpheart.00866.2008.
64. Linglart L, Gelb BD. Congenital Heart Defects in Noonan Syndrome: Diagnosis, Management, and Treatment. *Am J Med Genet C Semin Med Genet* (2020) 184(1):73-80. Epub 2020/02/06. doi: 10.1002/ajmg.c.31765.
65. Krenz M, Yutzey KE, Robbins J. Noonan Syndrome Mutation Q79r in Shp2 Increases Proliferation of Valve Primordia Mesenchymal Cells Via Extracellular Signal-Regulated Kinase 1/2 Signaling. *Circ Res* (2005) 97(8):813-20. Epub 2005/09/17. doi: 10.1161/01.RES.0000186194.06514.b0.
66. Blume C, Kraus X, Heene S, Loewner S, Stanislawski N, Cholewa F, et al. Vascular Implants - New Aspects for in Situ Tissue Engineering. *Eng Life Sci* (2022) 22(3-4):344-60. Epub 2022/04/07. doi: 10.1002/elsc.202100100.
67. Wissing TB, Bonito V, van Haaften EE, van Doeselaar M, Brugmans M, Janssen HM, et al. Macrophage-Driven Biomaterial Degradation Depends on Scaffold Microarchitecture. *Front Bioeng Biotechnol* (2019) 7:87. Epub 2019/05/14. doi: 10.3389/fbioe.2019.00087.
68. Tang D, Chen S, Hou D, Gao J, Jiang L, Shi J, et al. Regulation of Macrophage Polarization and Promotion of Endothelialization by No Generating and Peg-Yigsr Modified Vascular Graft. *Mater Sci Eng C Mater Biol Appl* (2018) 84:1-11. Epub 2018/03/10. doi: 10.1016/j.msec.2017.11.005.
69. Wynn TA, Ramalingam TR. Mechanisms of Fibrosis: Therapeutic Translation for Fibrotic Disease. *Nat Med* (2012) 18(7):1028-40. Epub 2012/07/10. doi: 10.1038/nm.2807.

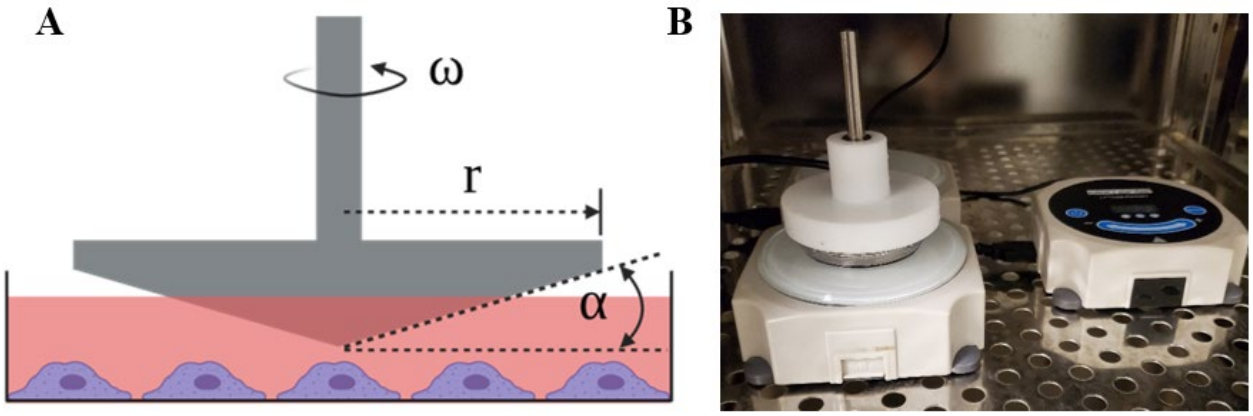

Figure 1. Cone-and-plate system. (A) Schematic of the cone-and-plate system where MDMs are attached to the bottom of the petri dish and a cone is loaded on top. (B) Setup of the cone-and-plate system in the incubator. The right side shows the controller that sets the RPM of the system.

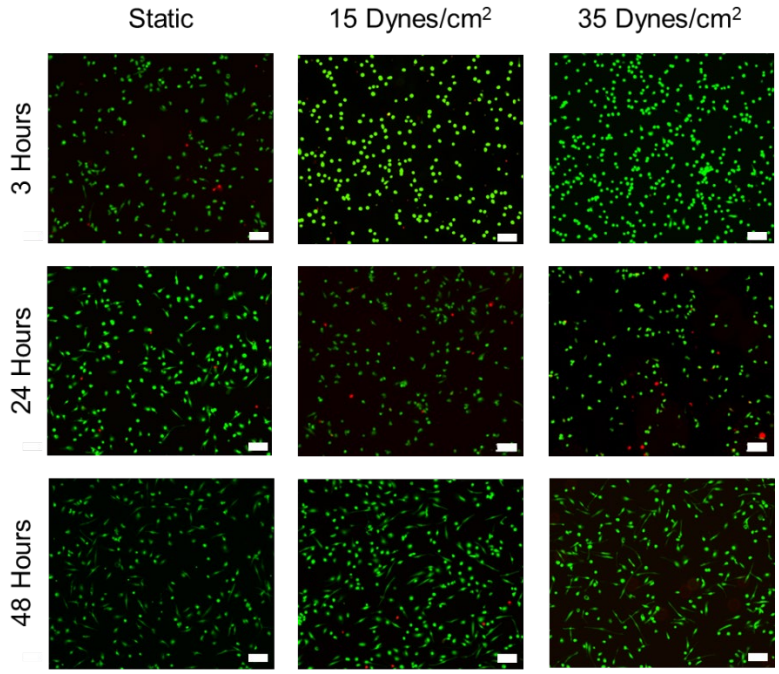

Figure 2. Live/dead staining following shear exposure. Each image was taken immediately after shear exposure at 3, 24, and 48 hours and is representative of all data collected. Scale bar = 100 μm.

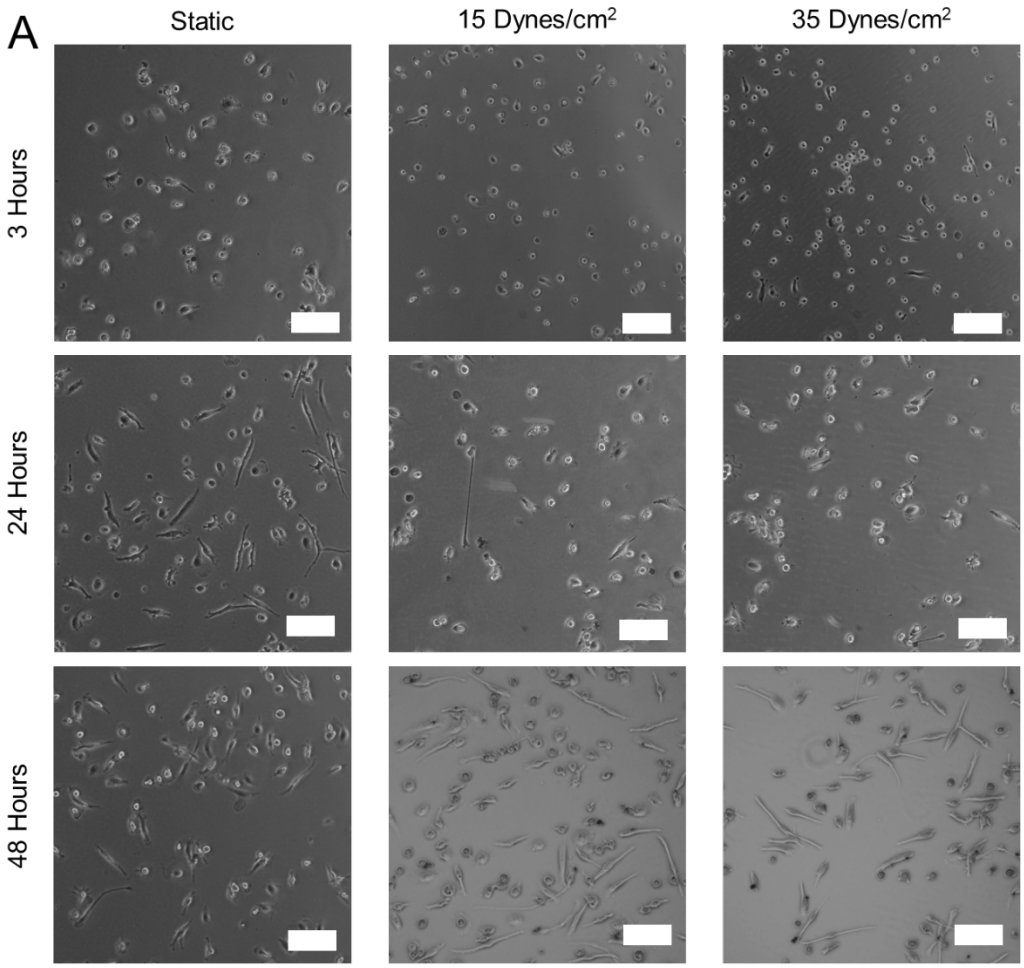
A
Static
15 Dynes/cm2
35 Dynes/cm2
3 Hours
24 Hours
48 Hours

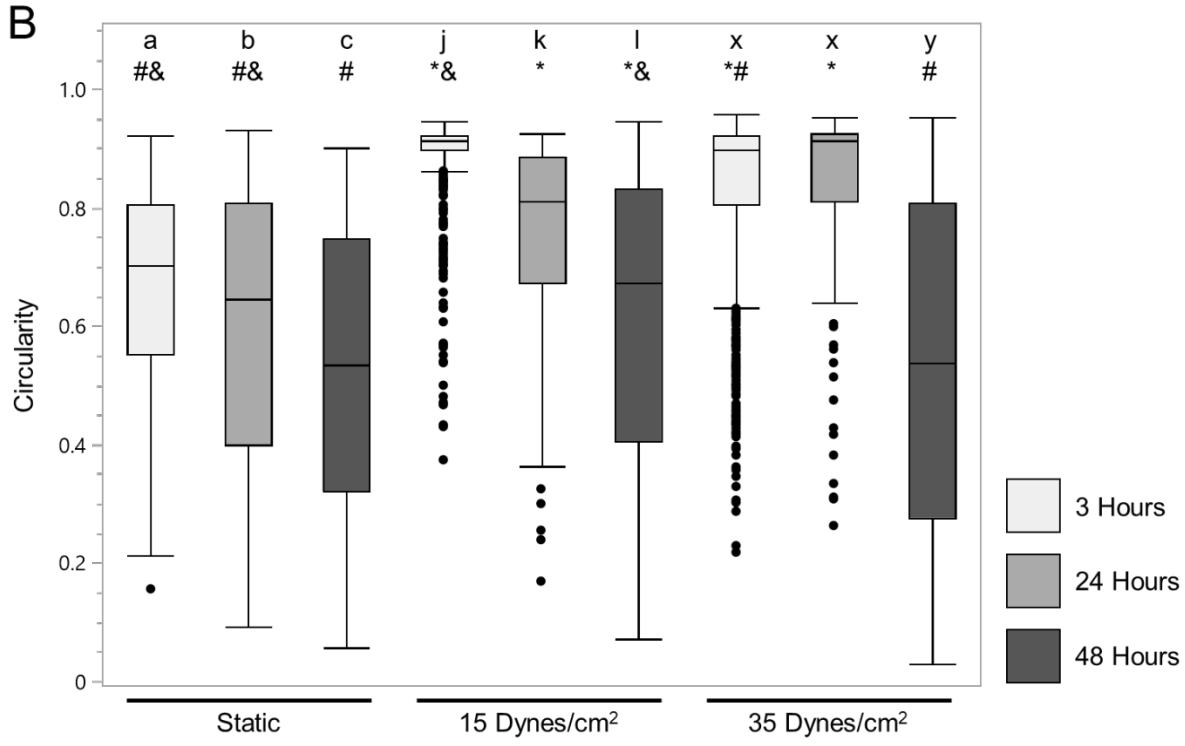
B
a
#&
b
#&
c
#
j
*&
k
*
l
*&
x
*#
x
*
y
#
Circularity
1.0
0.8
0.6
0.4
0.2
0
Static
15 Dynes/cm2
35 Dynes/cm2
3 Hours
24 Hours
48 Hours

Figure 3. (A) Brightfield imaging and (B) circularity analysis of MDM morphology after exposure to static, 15 dynes/cm^2, and 35 dynes/cm^2 conditions for a period of 3, 24, and 48 hours. Data is expressed as mean ± SD, n = ~500 for circularity analysis. Scale bar = 100 µm. Different letters indicate statistically significant differences between timepoints ($p < 0.05$) within a shear condition. Letter groups are as follows: a, b, c compares within the static condition; j, k, l compares within the 15 dynes/cm^2 condition; x, y, z compares within the 35 dynes/cm^2 condition. Statistically significant differences between timepoints among shear conditions are indicated by: *different from the same timepoint compared to the static condition; $^\#$different from the same timepoint compared to the 15 dynes/cm^2 condition; $^\&$different from the same timepoint compared to the 35 dynes/cm^2 condition.

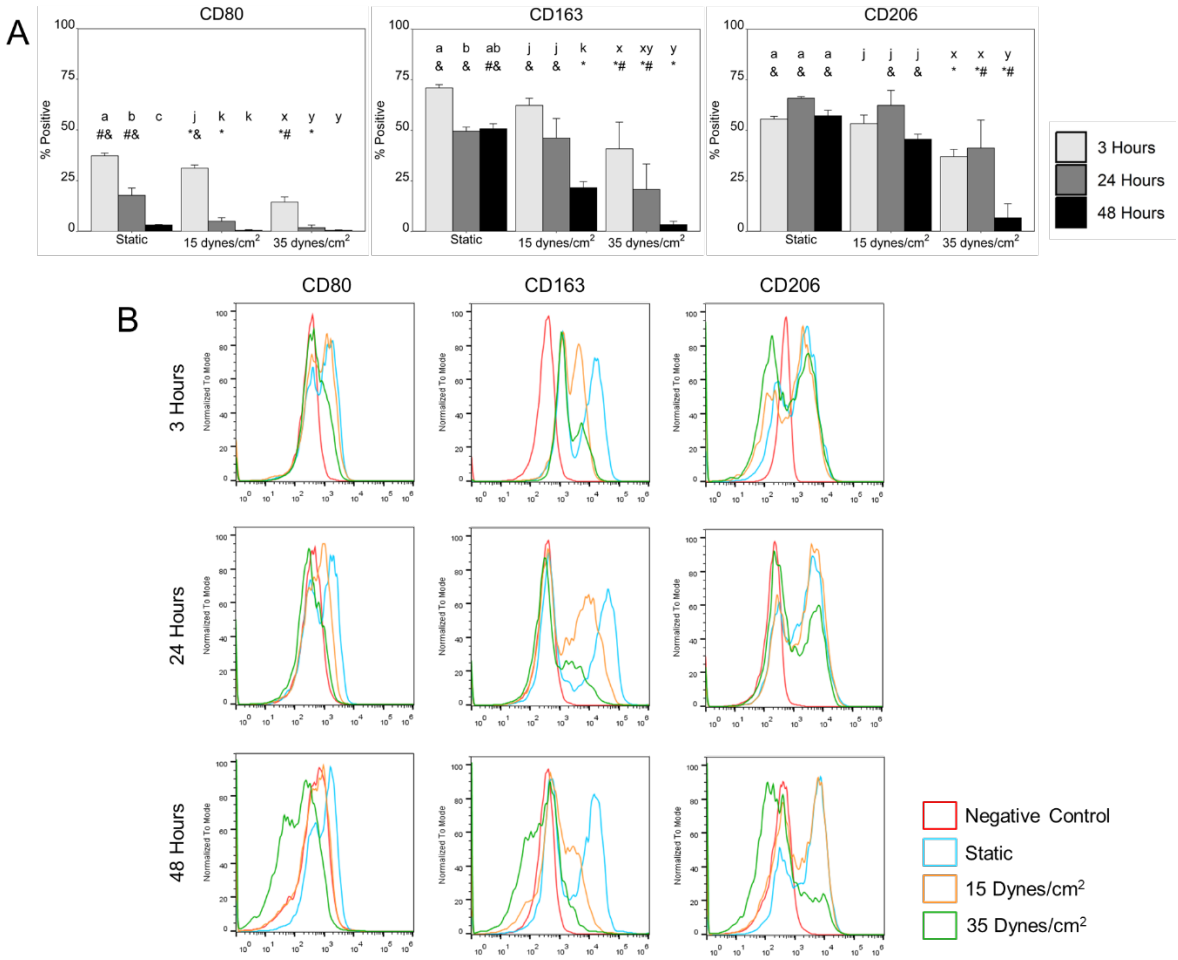

Figure 4. (A) Percent positive protein expression through flow cytometry. CD80, CD163, and CD206 expression was evaluated through flow cytometry following shear exposure. Data is represented as mean ± SD, n ≥ 3. Different letters indicate statistically significant differences between timepoints ($p < 0.05$) within a shear condition. Letter groups are as follows: a, b, c compares within the static condition; j, k, l compares within the 15 dynes/cm^2 condition; x, y, z compares within the 35 dynes/cm^2 condition. Statistically significant differences between timepoints among shear conditions are indicated by: *different from the same timepoint compared to the static condition; $^\#$different from the same timepoint compared to the 15 dynes/cm^2 condition;

[&]different from the same timepoint compared to the 35 dynes/cm^2 condition. (B) Flow cytometry histograms for CD80, CD163, and CD206 are shown for every timepoint (3, 24, and 48 hours). The data shown are from single samples representative of all data.

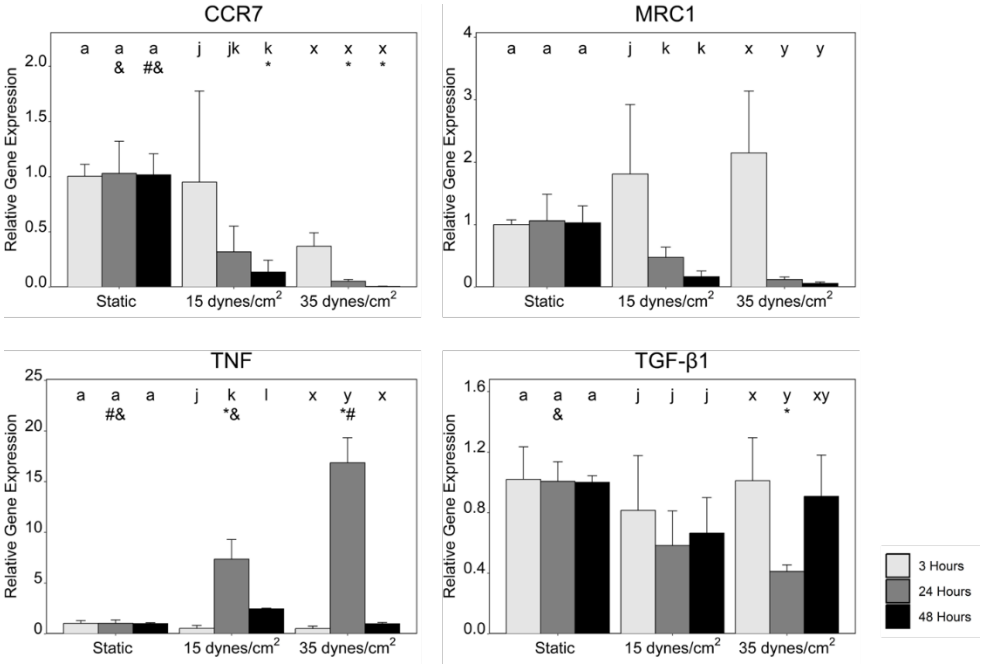

Figure 5. Gene expression of TNF, TGF-β, CCR7, and MRC1 from MDMs cultured under static, 15 dynes/cm^2, and 35 dynes/cm^2 conditions for a period of 3, 24, and 48 hours. Data is expressed as mean ± SD, n ≥ 3. Different letters indicate statistically significant differences between timepoints ($p < 0.05$) within a shear condition. Letter groups are as follows: a, b, c compares within the static condition; j, k, l compares within the 15 dynes/cm^2 condition; x, y, z compares within the 35 dynes/cm^2 condition. Statistically significant differences between timepoints among shear conditions are indicated by: [*]different from the same timepoint compared to the static condition; [#]different from the same timepoint compared to the 15 dynes/cm^2 condition; [&]different from the same timepoint compared to the 35 dynes/cm^2 condition.

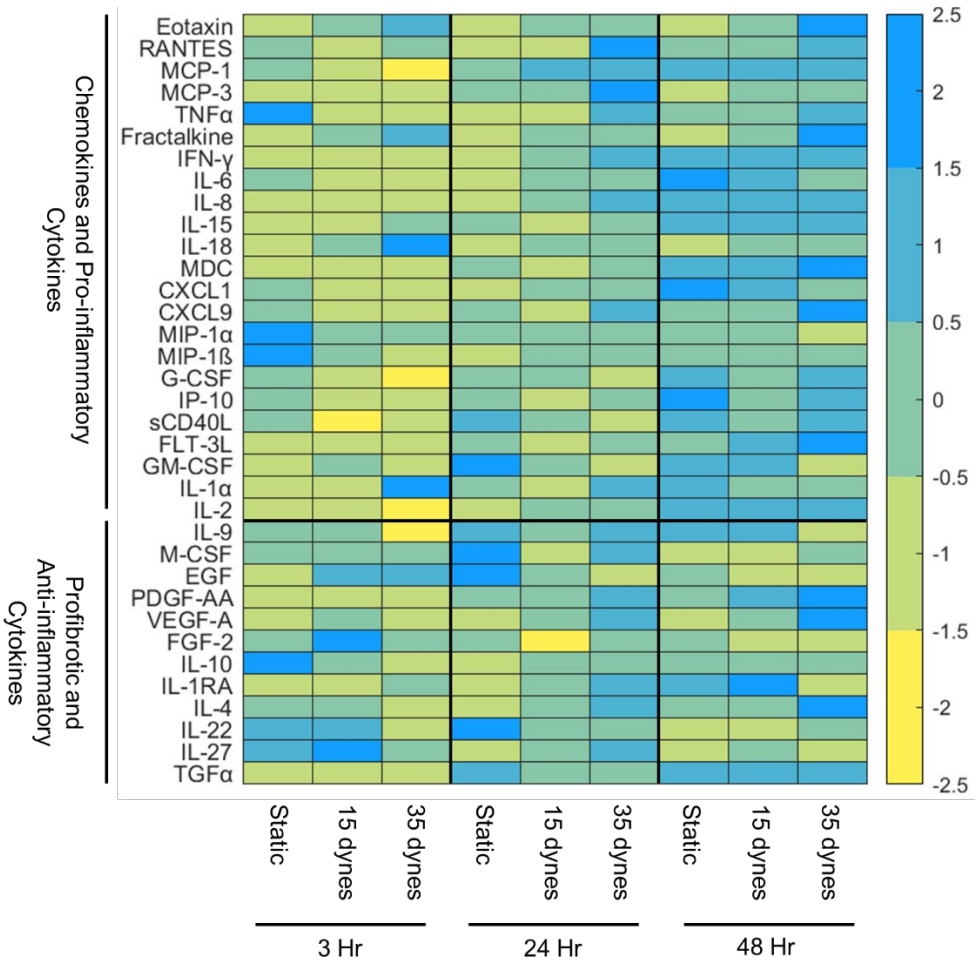

Figure 6. Heatmap of cytokines released by MDMs cultured under static, 15 dynes/cm^2, and 35 dynes/cm^2 conditions for a period of 3, 24, and 48 hours. Cytokine secretion level is represented using z-scores.

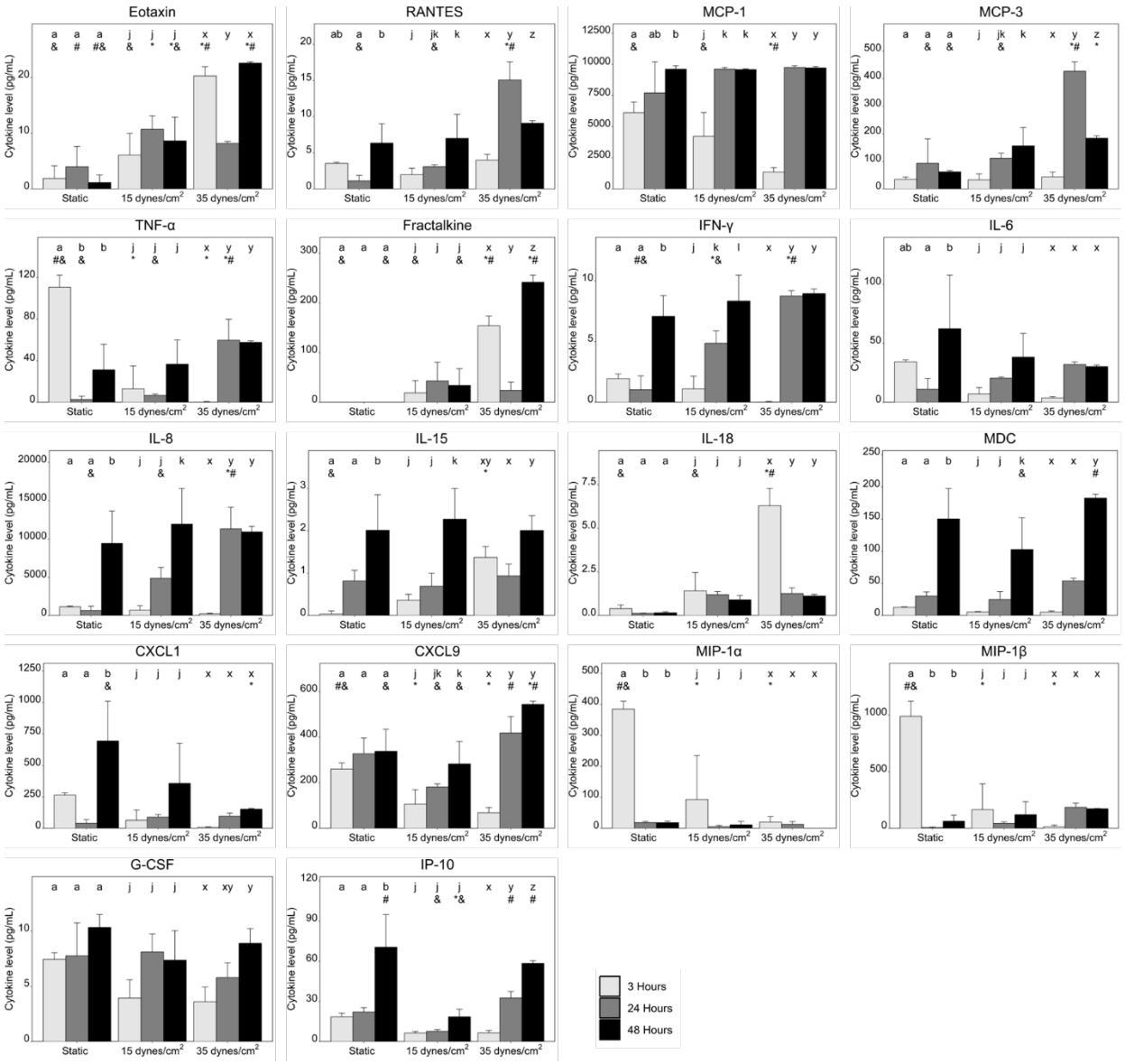

Figure 7. Chemokines and pro-inflammatory cytokine secretion from MDMs cultured under static, 15 dynes/cm^2, and 35 dynes/cm^2 conditions for a period of 3, 24, and 48 hours. Data is expressed as mean ± SD, n = 4. Different letters indicate statistically significant differences between timepoints ($p < 0.05$) within a shear condition. Letter groups are as follows: a, b, c compares within the static condition; j, k, l compares within the 15 dynes/cm^2 condition; x, y, z compares within the 35 dynes/cm^2 condition. Statistically significant differences between timepoints among shear conditions are indicated by: *different from the same timepoint compared to the static condition; $^\#$different from the same timepoint compared to the 15 dynes/cm^2 condition; $^\&$different from the same timepoint compared to the 35 dynes/cm^2 condition.

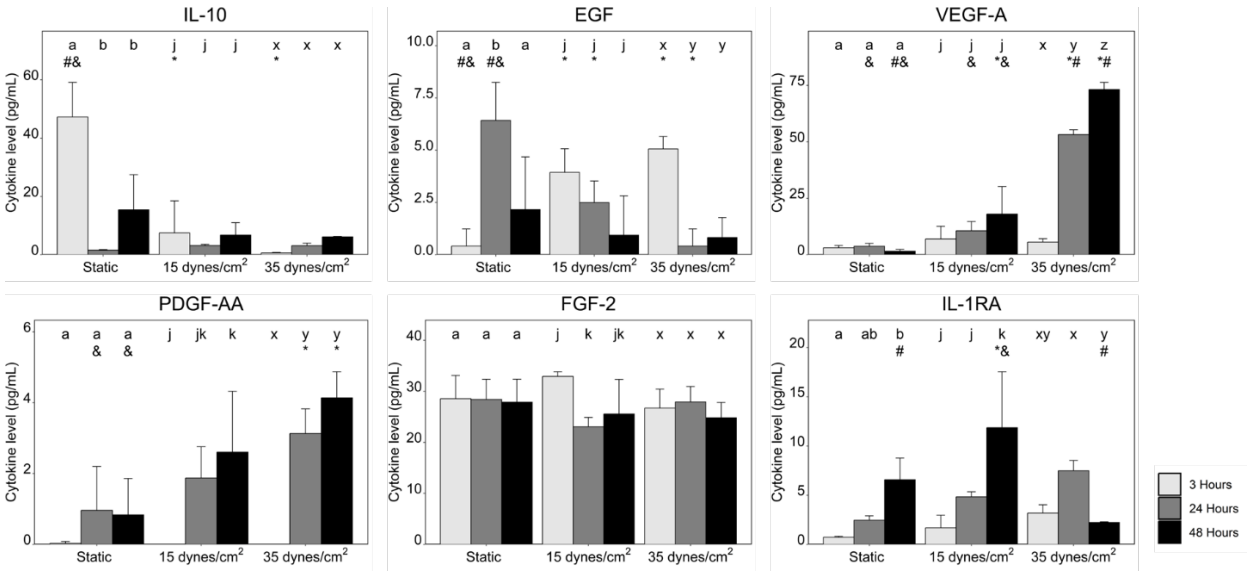

Figure 8. Anti-inflammatory cytokine secretion from MDMs cultured under static, 15 dynes/cm^2, and 35 dynes/cm^2 conditions for a period of 3, 24, and 48 hours. Data is expressed as mean ± SD, n = 4.

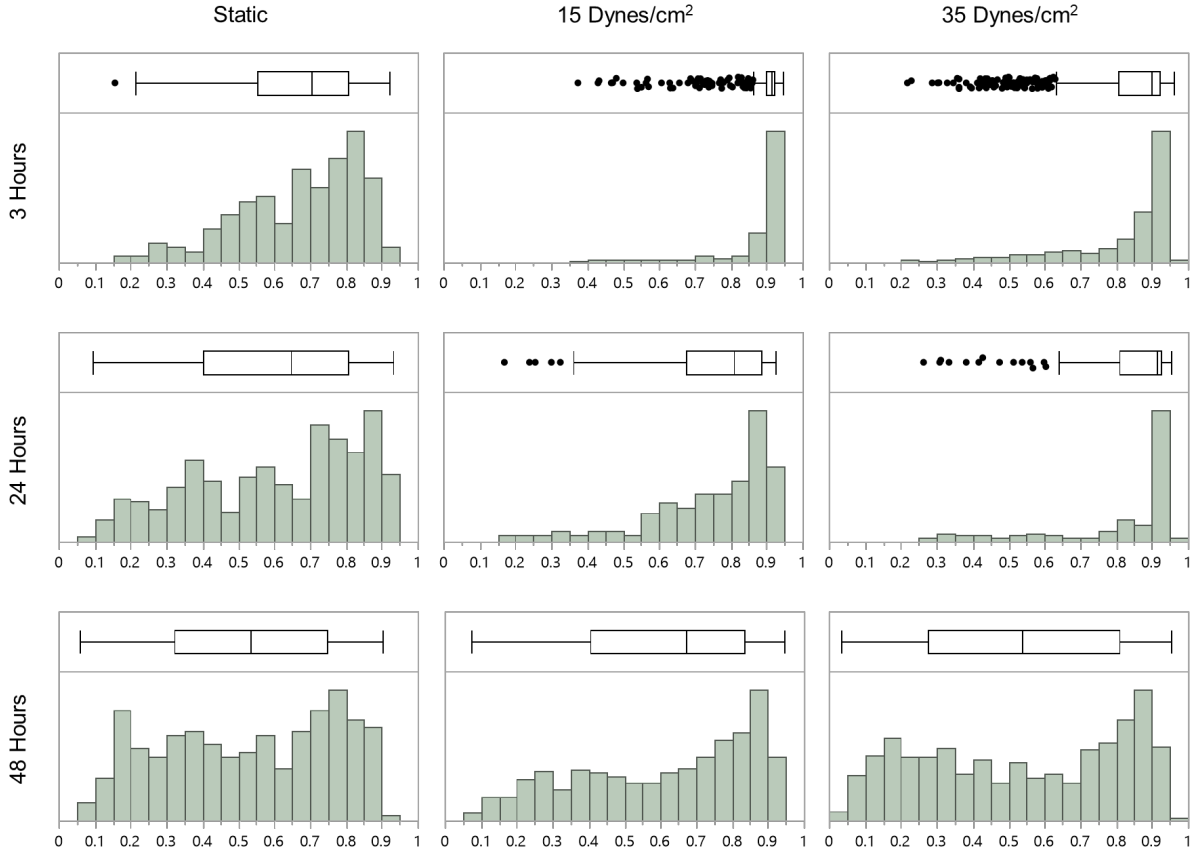

Supplemental Figure 1. Histograms and boxplots representing the circularity distribution of MDMs cultured under static, 15 dynes/cm^2, and 35 dynes/cm^2 conditions for a period of 3, 24, and

48 hours. The boxplots show the outliers, minimum, median, and maximum circularity for each group.